Desalination and Water Treatment
www.deswater.com
doi: 10.1080/19443994.2015.1063090

57 (2016) 14609–14621
July

Taylor & Francis
Taylor & Francis Group

Characterization and application of heat-treated and acid-leached halloysites in the removal of malachite green: adsorption, desorption, and regeneration studies

Fatiha Bessaha[a], Kheira Marouf-Khelifa[a], Isabelle Batonneau-Gener[b], Amine Khelifa[a,*]

[a]*Laboratoire de Structure, Elaboration et Applications des Matériaux Moléculaires (S.E.A.2M.), Département de Chimie, Université de Mostaganem, B.P. 981, R.P., Mostaganem 27000, Algeria, Tel. +213 45 21 60 80; Fax: +213 45 21 10 18; email: aminekhelifadz@yahoo.fr (A. Khelifa)*

[b]*Institut de Chimie des Milieux et Matériaux de Poitiers IC2MP (UMR 7285 CNRS), Université de Poitiers, 4 rue Michel Brunet, 86022 Poitiers, France*

Received 1 December 2014; Accepted 10 June 2015

ABSTRACT

Algerian halloysite was processed at 600°C and with 5-N HCl (H600-5N), and compared with the forms treated thermally at 600°C (H600) and unmodified (H). The obtained samples were characterized by FTIR, TEM, and nitrogen adsorption, and employed as malachite green (MG) adsorbents from aqueous solutions. The effects of pH, contact time, solution concentration, and temperature were examined. A particular attention has been focused on desorption and regeneration. The ease in desorption and regeneration constitutes a major practical advantage for treating industrial effluents. Thermo-chemical activation leads to the leaching of Al ions from the octahedral sheet. As consequence, H600-5N presents a specific area of 503 $m^2 g^{-1}$, i.e. eight orders of magnitude higher than that of H (63 $m^2 g^{-1}$). For all halloysitic solids, the capacity in MG increases with decreasing adsorption temperature. The affinity sequence is H600-5N > H600 > H. The isotherms are found to be well represented by the Redlich–Peterson equation. The thermodynamic data show that the MG adsorption onto H600-5N is spontaneous and exothermic, consequence of the electrostatic attraction between positively charged molecules and negatively charged adsorption sites. Among the seven eluents used, methanol manifests the greatest desorption capacity from H600-5N, which increases overall with temperature. After four adsorption–desorption cycles, this material was easily desorbed and regenerated. On the basis of all these considerations and, also, its adsorption capacity (192.6 mg g^{-1} at 25°C), H600-5N appears very effective for removing dyes from wastewaters.

Keywords: Halloysite; Modification; Removal; Malachite green; Desorption; Regeneration

1. Introduction

Synthetic dyes are extensively used in various industries such as textile, paper, rubber, plastic, leather, cosmetic, food, and pharmaceutical. After use, they are generally released into effluents. Color is the first contaminant to be recognized in these effluents. The presence of very small amounts of dyes in water is highly discernible and undesirable [1], and

*Corresponding author.

generates huge problems for the environment and living organisms because they are recalcitrant organic molecules, resistant to aerobic digestion, stable to light, heat, and oxidizing agents [2].

Among these dyes, malachite green (MG), a basic dye, is widely used for dyeing of cotton, silk, leather, wool, jute, paper, and as a food additive [3]. When MG is discharged into wastewaters, it affects the aquatic life and is found to be toxic to human and animal cells [4]. After use, different techniques have been used to treat this contaminant: biological treatment [5], photodegradation [6], decolorization [7], and coagulation–flocculation [8]. These processes suffer from a certain number of problems such as partial degradation, high cost, and optimization of the operational parameters. Adsorption is an effective and clean technique for removing pollutants from wastewater of the textile, paper, and allied industries [9]. To make this process ecologically and economically feasible, the saturated samples must be regenerated for restoring their adsorption capacities. The reusability of adsorbent constitutes a key factor in industrial chemical engineering. Regeneration can be achieved with solvents or aqueous solutions of acids, bases, or salts.

Different adsorbents were used to fix MG from aqueous solutions, such as nanocomposites [10], sawdust [11], activated carbon [12,13], and polymers [14]. These materials were found to be costly in addition to disadvantages due to their subsequent treatment and regeneration. These limitations have oriented the investigations for inexpensive and readily available materials. If kaolinite received a great interest from the scientific community, little research has considered modified halloysites. Halloysite belongs to the same family as kaolinite, i.e. the kaolin group, but differs by having a hollow microtubular structure [15].

The objective of this paper is to evaluate the potential of the modified halloysites for removing MG from aqueous solutions. Three halloysitic solids were considered, viz. unmodified halloysite (H), the form processed at 600˚C (H600), and that treated at 600˚C and with 5-N HCl (H600-5N). Before adsorption, the materials were characterized by FTIR, TEM, and nitrogen adsorption. The effects of pH, contact time, solution concentration, and temperature were examined. A particular attention has been focused on the desorption of MG and the regeneration of the best adsorbent. Desorption was considered by varying temperature and via seven solvents, such as water, methanol, acetone, DMSO… The regeneration of H600-5N was studied through six consecutive cycles, to investigate the economic feasibility of using this heat-treated and acid-leached halloysite as industrial adsorbent.

2. Materials and methods

2.1. Materials

Raw halloysite from Djebel Debbagh, Guelma (eastern region of Algeria) was used in this work. Its characteristics were reported in a previous work [16]. Its chemical composition in mass % is SiO_2: 46.34; Al_2O_3: 37.96; Fe_2O_3: 0.05; CaO: 0.83; MgO: 0.08; K_2O: 0.02; Na_2O: 0.02; MnO_2: 1.25; loss on ignition (1,000˚C for 1 h): 13.45%.

Three hundred grams of the starting material were heated at 600˚C for 2 h in air atmosphere, at a rate of 10˚C min^{-1}, to make sure that this clay dehydroxylates [17]. It is well known that 2 h is a time sufficient so that heat penetrates into the interior of the particles and induces some transformations, for a certain number of materials [18,19].

Acid activation was carried out by mixing 45 g of halloysite treated at 600˚C with 1,125 mL of HCl solution (solid/solution ratio: 1/25) of concentration 5 N. The suspension was stirred at 70˚C for 4 h then filtered. The recovered solid was abundantly washed with distilled water, to remove any unspent acid, dried at 110˚C for 2 h, and stored for further use. The samples were named H, H600, and H600-5N, respectively.

2.2. Characterization

The chemical analysis of the untreated halloysite and the SiO_2/Al_2O_3 molar ratio of all halloysitic solids were determined by ICP-AES on a Perkin-Elmer instrument. Infrared spectra were recorded with a Shimadzu 1240 FT-IR spectrometer (resolution 2 cm^{-1}). The structure band region (4,000–400 cm^{-1}) was investigated using KBr wafers containing 0.5% of sample. TEM images were determined with a JEOL 2100 electron microscope. An EDX detector for X-ray energy dispersive analysis was attached to this microscope. The clay sample was previously ultrasonically dispersed in ethanol for 5 min. The assessment of textural properties was carried out by nitrogen adsorption–desorption. The measurements were performed at 77 K via an ASAP 2010 instrument (Micromeritics). Specific surface area was calculated by the BET method. External surface area and micropore volume were determined by the *t*-plot method. Mesopore volume was calculated from the desorption branch of the corresponding nitrogen isotherm.

2.3. Adsorption procedure

A stock solution of MG (C.I.: 42555, chemical formula $C_{52}H_{54}N_4O_{12}$, FW: 927.00 g mol^{-1}, λ_{max} = 617 nm,

supplied by Merck) of concentration 1,000 mg L^{-1} was prepared by dissolving an appropriate amount in distilled water. The working solutions were prepared by diluting the stock solution into the desired concentrations. The adsorption experiments were performed via the batch method. 0.02 g of the halloysitic solid was mixed with 20 mL of aqueous MG solution. After each experiment, the solution was separated by centrifugation. The supernatant was analyzed by visible spectrophotometry, at 617 nm, using a Shimadzu 1240 UV–vis spectrophotometer. The adsorbed amount was calculated from the difference between the initial and final concentrations. The effects of pH, contact time, concentration, and temperature were studied. The experimental conditions are outlined in Table 1.

2.4. Theoretical considerations

2.4.1. Adsorption kinetics

In order to investigate the controlling mechanism of the adsorption process, various kinetic equations were applied to test the experimental data. Lagergren [20] proposed a pseudo-first-order kinetic model. The integral form of the model is

$$\log(Q_e - Q_t) = \log Q_e - \frac{K_1 t}{2.303} \quad (1)$$

where Q_t is the amount adsorbed at time t (mg g^{-1}), Q_e the adsorption capacity at equilibrium (mg g^{-1}), K_1 the pseudo-first-order rate constant (min^{-1}), and t is the contact time (min).

The adsorption kinetics may also be described by a pseudo-second-order reaction. The linearized-integral form of the model is [21]:

$$\frac{t}{Q_t} = \frac{1}{K_2 Q_e^2} + \frac{t}{Q_e} \quad (2)$$

where K_2 (g mg^{-1} min^{-1}) is the pseudo-second-order rate constant of adsorption. The initial adsorption rate, h, as $t \to 0$, can be defined as

$$h = K_2 \cdot Q_e^2 \quad (3)$$

The plot of t/Q_t vs. t should give a linear relationship, from which K_2 and h can be determined from the slope and intercept of the plot.

During adsorption under batch mode, there is a possibility of transport of adsorbate species into the pores of adsorbent, which is often the rate-controlling step. The intraparticle diffusion rate equation can be written as follows [22]:

$$Q_t = K_{id} t^{1/2} + C \quad (4)$$

where K_{id} (mg g^{-1} $min^{-1/2}$) is the intraparticle diffusion rate constant and C is the constant. The values K_{id} and C are calculated from the slope and the intercept, respectively, of the plot of Q_t vs. $t^{1/2}$.

Kasra equation, introduced by Samiey and Farhadi [23], can be abbreviated as:

$$Q_t = At^2 + Bt + C \quad (5)$$

where

$$A = \frac{1}{2}a_i,\ B = v_{0i} - a_i t_{0i} \text{ and } C = Q_{0i} - \frac{1}{2}a_i t_{0i}^2 - (v_{0i} - a_i t_{0i}) \cdot t_{0i} \quad (6)$$

with a_i: adsorption acceleration; v_{0i} and t_{0i}: velocity and time values in the beginning ith region, respectively; v_i: Adsorption velocity in the ith region at time t.

Table 1
Experimental conditions during the adsorption/desorption of MG

Contact time	1, 3, 5, 10, 20, 40, 60, 120, 240 min; $C_{initial}$ = 80 mg L^{-1} [Solid]/[solution]: 1 g L^{-1}; T: 25, 40, 55°C; pH: 5.1
Concentration	40, 60, 80, 100, 150, 200, 300, 400 mg L^{-1} [Solid]/[solution]: 1 g L^{-1}; contact time: 2 h; pH: 5.1
Temperature	25, 40, 55°C [Solid]/[solution]: 1 g L^{-1}; contact time: 2 h; pH: 5.1
pH	pH 3.1–5.0–6.9–9.0; $C_{initial}$ = 80 mg L^{-1} [Solid]/[solution]: 1 g L^{-1}; contact time: 2 h; T: 25°C
Desorption	Solvents: water (H_2O); methanol (CH_3OH); ethanol (C_2H_6O); butanol ($C_4H_{10}O$); DMSO (dimethylsulfoxide); acetone (C_3H_6O); 50% (water) + 50% (methanol) [Solid]/[solution]: 1 g L^{-1}; contact time: 4 h; T: 25, 55°C $C_{initial}$ = 400 mg L^{-1}

2.4.2. Adsorption isotherms modeling

The equilibrium models of Langmuir, Freundlich, and Redlich–Peterson (RP) were used to fit the experimental data. The Langmuir equation can be written under the following form [24]:

$$\frac{C_e}{Q_e} = \frac{1}{Q_m \cdot K_L} + \frac{C_e}{Q_m} \quad (7)$$

where Q_e is the equilibrium amount removed from solution (mg g^{-1}), C_e is the equilibrium concentration (mg L^{-1}), K_L is the constant related to the affinity of binding sites (L mg^{-1}), and Q_m is the maximum amount per unit weight of adsorbent for complete monolayer coverage (mg g^{-1}).

The Freundlich model has been widely adopted and may be written under the form [25]:

$$\log Q_e = \log K_F + \frac{1}{n} \log C_e \quad (8)$$

where K_F is the constant taken as an indicator of adsorption capacity (L g^{-1}) and $1/n$ is the constant indicative of the adsorption intensity.

The three-parameter RP equation [26] has been proposed to improve the fit by the Langmuir or Freundlich equations and is given by:

$$Q_e = \frac{K_{RP} C_e}{1 + a_{RP} C_e^{\beta}} \quad (9)$$

where Q_e (mg g^{-1}) is the amount adsorbed at equilibrium, C_e (mg L^{-1}) is the equilibrium solution concentration, K_{RP} and a_{RP} are the constants of the RP equation, and β is the heterogeneity factor that depends on surface properties of the adsorbent.

2.4.3. Thermodynamic study

The thermodynamic parameters ΔH°, ΔS°, and ΔG° were evaluated using the equation:

$$\ln K_d = (-\Delta H^\circ / R \cdot T) + (\Delta S^\circ / R) \quad (10)$$

where ΔH° and ΔS° are the change in enthalpy (kJ mol^{-1}) and entropy (J mol^{-1} K^{-1}), respectively. T is the absolute temperature (K), R is the gas constant (J mol^{-1} K^{-1}), and K_d is the distribution coefficient (L g^{-1}). This coefficient reflects the overall MG-surface affinity and is given by:

$$K_d = Q_e / C_e \quad (11)$$

The enthalpy and entropy changes are graphically determined by plotting ln K_d vs. $1/T$, which gives a straight line. According to thermodynamics, the Gibbs free energy change, ΔG°, is related to ΔH° and ΔS° at constant temperature by the following equation:

$$\Delta G^\circ = \Delta H^\circ - T\Delta S^\circ \quad (12)$$

3. Results and discussion

3.1. Characterization

3.1.1. FTIR analysis

The FTIR spectra are shown in Fig. 1. The starting material, H, highlights two bands in the 3,700–3,600 cm^{-1} region, characteristic of the stretching vibrations of hydroxyl groups. The vibration at 1,115 cm^{-1} is assigned to the stretching mode of apical Si–O. The bands at 1,042 and 922 cm^{-1} are caused by the stretching vibrations of Si–O–Si and the bending mode of inner surface hydroxyl groups, Al–O–H, respectively [27]. The band observed at 548 cm^{-1} is due to the deformation vibration of Al–O–Si. A detailed assignment was previously given [16]. When halloysite is processed at 600°C (H600), significant changes occur in the vibrational spectrum. The 3,704 and 3,632 cm^{-1} bands disappear, indicating a release of OH radicals, due to the dehydroxylation of structural aluminol groups [17]. The 922 cm^{-1} band due to Al–O–H also vanishes, implying once again aluminol groups.

After heat treatment and acid activation, a broad band in the 3,100–3,700 cm^{-1} range with a maximum at 3,429 cm^{-1} appears in the H600-5N spectrum, indicating the formation of silica nanoparticles [28]. The signal at 1,115 cm^{-1}, corresponding to the stretching mode of apical Si–O, disappears. As this oxygen binds silicon to aluminum of octahedral sheet, the latter is disturbed by acid attack. The widening of the band having a maximum at 1,077 cm^{-1}, the disappearance of the signals at 682 (Si–O–Al) and 760 cm−1 (Si–O–Al perpendicular stretching), and the increase in the 794 cm^{-1} band (symmetric Si–O–Si stretching; 780 cm^{-1} in H), indicate the formation of amorphous silica [29] and the depopulation of octahedral sheet, subsequent to the dissolution of alumina [28]. In line with this interpretation, the SiO_2/Al_2O_3 molar ratio rises from 2.08 (H) to 27.11 (H600-5N) (Table 2).

3.1.2. Transmission electron microscopy

TEM images of H, H600, and H600-5N are presented in Fig. 2. The starting material, H, evidences

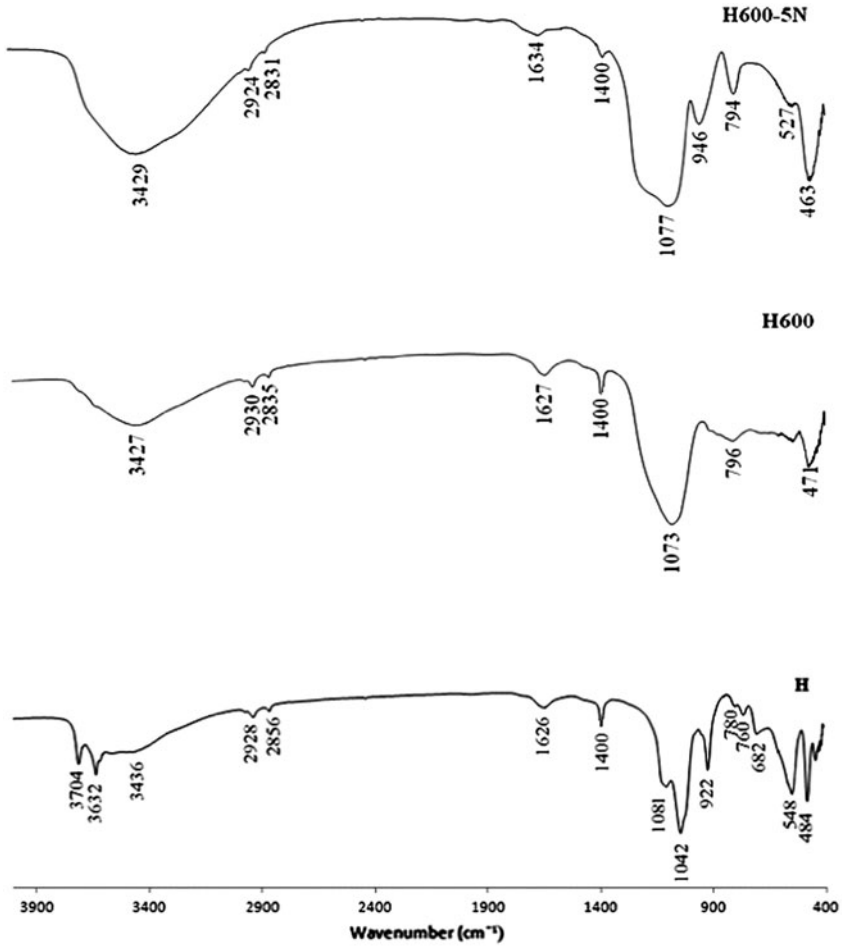

Fig. 1. FTIR spectra of H, H600, and H600-5N.

particles having a cylindrical shape and contains a transparent central area that runs longitudinally along the cylinder, indicating that the nanotubular particles are hollow and open-ended. The particles are of rather different sizes both in diameter and in length. Their external diameters vary from 50 to more than 100 nm while internal diameter is about 10 nm. These rolled tubes consist in a number of aluminosilicate sheets, curved, and closely packed. Nanotubular particles were also obtained for H600 proving that the thermal treatment at 600°C conserves the morphology of halloysite. Their external and internal diameters vary from 30 to 180 nm and from 10 to 30 nm, respectively. A phase rich in Al, O, and Mn was evidenced by EDX in the microscope. This phase consists of agglomerated small plates of diameter about 10 nm. H600-5N also leads to a tubular morphology, although the obtained tubes are damaged. Dehydroxylation phenomenon associated with the leaching of Al^{3+} alters somewhat the tubular shape of halloysitic clays. The observation of these morphological details is of a great relevance. The defects on surface such as surface breakage or crystallographic defects could prove as potential reaction sites for the surface chemistry of halloysite nanotubes [30].

3.1.3. Textural analysis

The textural parameters are summarized in Table 2. Specific surface area, S_{BET}, remains more or less constant after thermal treatment at 600°C. As the unmodified halloysite, the texture of H600 is primarily represented by mesopores, with 98% of the total volume of pores. This confirms the mesoporous character of dehydroxylated halloysite. Thermo-chemical activation leads to a specific surface area of 503 $m^2 g^{-1}$ for H600-5N, i.e. eight orders of magnitude higher than that of H (63 $m^2 g^{-1}$). This increase is accompanied by that of internal and external surfaces, in a ratio of 27.7 and 2.9, respectively. This shows that the leaching

Table 2
SiO_2/Al_2O_3 molar ratio and textural parameters of the modified halloysites

Samples	SiO_2/Al_2O_3 molar ratio	Specific surface area S_{BET} ($m^2\ g^{-1}$)	External surface area S_{ext} ($m^2\ g^{-1}$)	Internal surface area S_{int} ($m^2\ g^{-1}$)	Total volume of pores ($cm^3\ g^{-1}$)	Micropore volume ($cm^3\ g^{-1}$)	Mesopore volume ($cm^3\ g^{-1}$)	$\frac{\text{Micropore volume}}{\text{Total volume}} \times 100$ (%)
H	2.08	63	50.1	12.9	0.288	0.006	0.282	2.1
H600	1.92	60.5	48.9	11.6	0.273	0.005	0.268	1.8
H600-5N	27.11	503.3	146.3	357.0	0.750	0.152	0.597	20.3

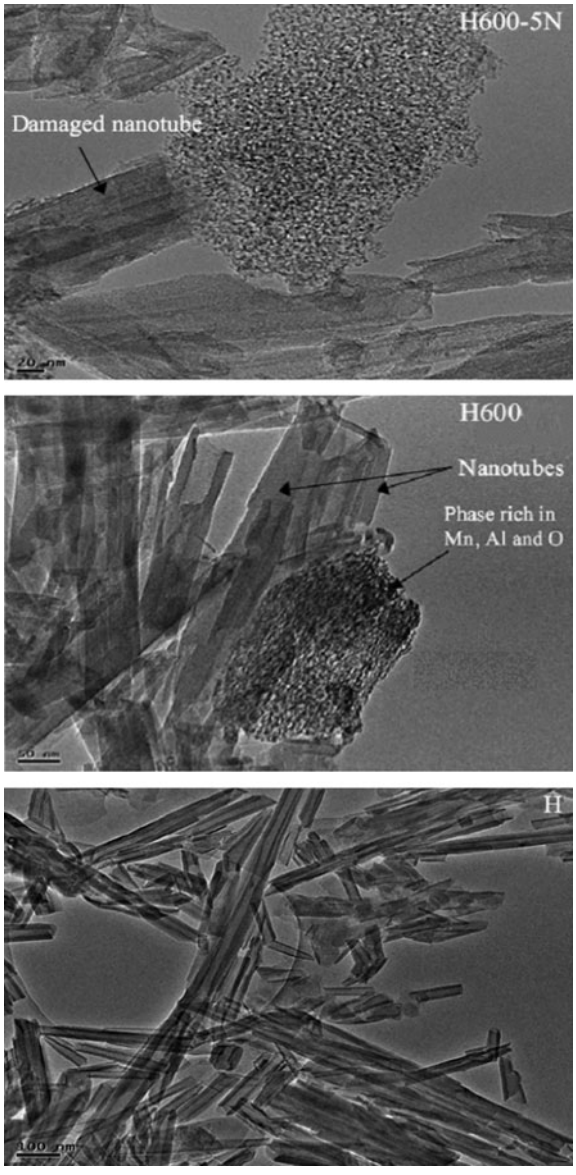

Fig. 2. Transmission electron microscopy images of H, H600, and H600-5N.

phenomenon increases mainly the internal surface of the material. Chemical activation extracts Al^{3+} cations from the octahedral sheet, destroys fragments of layers, causes the formation of "holes" in the halloysitic matrix, and ensures the accessibility of internal surface. In line with this behavior, microporosity and the SiO_2/Al_2O_3 molar ratio rise up to 20.3% and 27.11, respectively (Table 2).

3.2. MG adsorption

3.2.1. pH influence

The effect of pH is shown in Fig. 3 at $C_{initial} = 80\ mg\ L^{-1}$. The MG^+ adsorption increases quickly from pH 3 to 5, beyond which it remains more or less constant. Hameed and El-Khaiary [31] also obtain such an evolution, in the case of the fixing of green malachite by wood. For illustration, H600-5N adsorbs 32.3 and 58.3 mg g^{-1} at pH 3 and 5, respectively. As mentioned in a previous work [16], Algerian halloysite has an isoelectric point (IEP) equal to 2.5. Its surface charge is positive at pH < 2.5 and negative for pH > 2.5. In the range 3–5, i.e. pH > pHiep, it must be expected that the retention ability increases with increasing the initial pH of the solution, consequence to the electrostatic attraction between the dye molecules, positively charged, and negatively charged adsorption sites. Adsorption does not vary significantly in the range of 5–9, because the accumulation of MG cations in the interfacial region causes the development of a positive charge, which inhibits further adsorption of MG cations [32].

3.2.2. Kinetic study

The effects of contact time and temperature are represented in Fig. 4. Adsorption rate is rapid in the first 10 min [33]. Thereafter it decreases gradually, reaching equilibrium at about 1 h. Further increase in contact time did not change significantly dye removal.

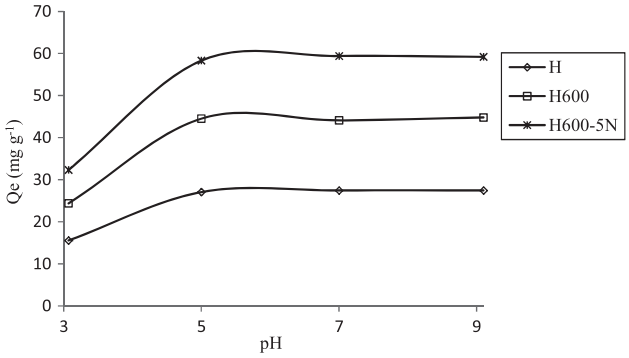

Fig. 3. Effect of initial pH on the adsorption of MG onto H, H600, and H600-5N.

So, an agitation time of 2 h seems to be sufficiently long to achieve equilibrium. Fast adsorption at the initial contact time is due to the availability of the negatively charged surface sites. The data also indicate that there is a significant difference in the removal of MG over the first 10 min. At 25˚C, H600-5N, H600, and H adsorb 80, 40, and 56% of their maximum capacity, respectively. The highest capacity of H600-5N is probably due to the accessibility of its internal surface. The decrease in adsorbed quantity with increasing temperature suggests a mechanism of physical nature.

The parameters of the models used are reported in Table 3. The pseudo-first-order equation was found unsuitable for H600-5N. The determination coefficients, R^2, are low, and the estimated theoretical quantities, Q_e (cal), are different from the experimental values, Q_e (exp). The fit of the experimental data with the pseudo-second-order model is more appropriate. Linear plots of t/Q_t vs. t (Eq. (2)) [21] were obtained (data not shown), corresponding to high R^2 values, i.e. >0.99. The Q_e (cal) and Q_e (exp) values are in close agreement. This model was successfully applied for the MG-eucalyptus bark system [34], and suggests that adsorption depends on the adsorbate–adsorbent couple.

The initial adsorption rate, h, decreases with increasing temperature, so that adsorption is hampered at first. The evolution of rate constants, K_2, as a function of temperature is unclear, indicating that the MG adsorption onto modified halloysites does not follow only second-order mechanism. The possibility of the intraparticle pore diffusion of adsorbate is always present especially for a porous material such as H600-5N. The plots of Q_t vs. $t^{1/2}$ (Eq. (4)) led to three linear portions (figures not shown). The first represents the external transport of mass, the second intraparticle diffusion, and the last surface saturation [22]. Except for H600 at 25˚C, high determination coefficients

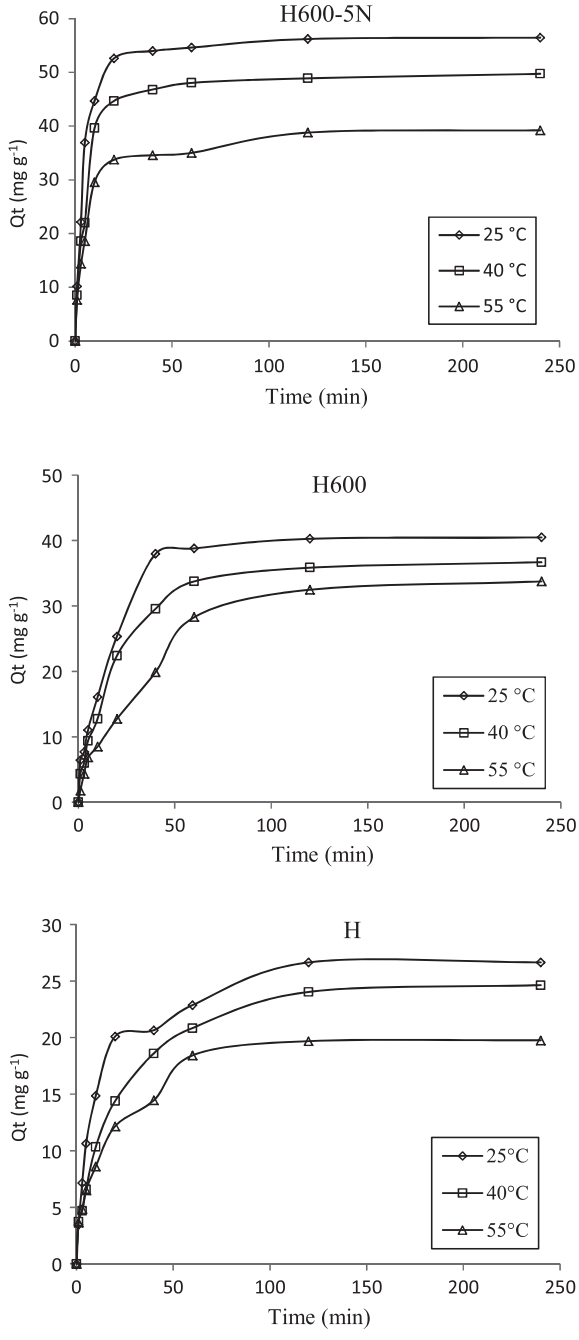

Fig. 4. Effect of contact time on the uptake of MG onto H, H600, and H600-5N, at 25, 40, and 55˚C.

(0.979–0.999) were obtained (Table 3), corresponding to the second linear portion. The intraparticle diffusion rate constant, K_{id}, decreases overall with temperature, indicating a hindrance in pore diffusion. Intraparticle diffusion cannot be accepted as the only rate-controlling step, due to the deviation of the plots from the origin (C values $\neq 0$, Table 3). As consequence, the boundary layer diffusion affects the MG adsorption to

Table 3
Kinetic parameters for MG adsorption onto modified halloysites

Samples	T (°C)	Pseudo-first-order model				Pseudo-second-order model				Intraparticle diffusion model			
		Q_t (exp) (mg g^{-1})	Q_t (cal) (mg g^{-1})	K_1 (min^{-1})	R^2	Q_t (cal) (mg g^{-1})	K_2 (g mg^{-1} min^{-1})	h (mg g^{-1} min^{-1})	R^2	K_{id} (mg g^{-1} min$^{-1/2}$)	C (mg g^{-1})	R^2
H	25	26.65	19.81	0.030	0.870	27.70	0.0013	3.10	0.999	6.12	0.75	0.996
	40	24.04	20.78	0.032	0.990	26.04	0.0015	1.94	0.998	4.19	0.38	0.999
	55	19.69	17.53	0.040	0.960	20.79	0.0023	1.91	0.997	2.91	1.97	0.999
H600	25	40.26	39.17	0.059	0.970	42.74	0.0020	4.02	0.997	4.24	7.79	0.854
	40	35.84	34.67	0.045	0.996	39.22	0.0018	2.77	0.997	3.49	7.00	0.994
	55	32.48	32.36	0.031	0.956	38.02	0.0009	1.37	0.991	2.48	6.15	0.841
H600-5N	25	56.19	31.41	0.059	0.843	57.14	0.0060	19.59	0.999	0.62	49.87	0.981
	40	48.88	32.36	0.065	0.921	50.76	0.0047	12.01	0.999	1.03	40.11	0.995
	55	38.78	23.44	0.038	0.757	40.00	0.0049	7.84	0.999	0.39	32.04	0.987

some extent. The values of intercept, C, give an idea about the thickness of boundary layer, i.e. the larger the intercept, the greater is the boundary layer effect [35]. The C values of H600-5N rise considerably compared to those of the unmodified halloysite. At 55°C, it is 59.3 times larger than that of H. Treatment with HCl disrupts the interfacial properties of dehydroxylated halloysites, so that the boundary layer effect plays a prominent role.

Kinetics of MG adsorption at different temperatures was studied by Kasra equation (Eq. (5)) [23], which shows that there are two regions before a plateau (data not shown). In each kinetic experiment, the number of surface adsorption sites and MG concentration decrease with increasing time. The values of acceleration, a_i, are globally negative, while velocity, v_i, decreases with increasing temperature (Table 4). For all materials, v_{0i} decreases and a_i becomes less negative from the first to the second region. This is due to the decrease in MG concentration and the number of unoccupied sites on the surface of the samples. The R^2 values are <0.91, so this equation cannot describe the adsorption kinetics of MG onto the modified halloysites.

3.2.3. Adsorption equilibrium

3.2.3.1. Isotherms. The adsorption equilibrium of MG onto H, H600, and H600-5N, was studied via a bath process at 25, 40, and 55°C. The isotherms are depicted in Fig. 5. Over the temperature range studied, the isotherms show that the extent of adsorption decreases with increasing temperature, indicating that a low temperature favors the MG removal from aqueous solutions. For example, H600-5N adsorbs 192.6 and 144.9 mg g^{-1} at 25 and 55°C, respectively. This feature suggests that the mechanism involves a physical process. Whatever temperature, the affinity follows the sequence H600-5N > H600 > H. The textural properties of H600-5N explain its highest capacity. The intermediate adsorption of H600, compared to H, is due to the amorphization of the structure, consequence of dehydroxylation phenomenon, which highlights a large degree of structural disorder [36]. Using the classification of Giles et al. [37], the obtained isotherms are L-shaped. The initial curvature of L-curve shows that the contaminant has a high affinity for the surface, while the slope falls steadily with a rise in concentration.

3.2.3.2. Comparison with other adsorbents. The values of the maximum adsorption capacity of different adsorbents towards MG are listed in Table 5. The results show that H600-5N has a great capacity because higher than for adsorbents such as kaolinite, zeolite,

Table 4
Coefficients and experimental te, Q_e, t_{02}, and Q_{02} values of Kasra equation for the kinetics of MG adsorption onto the modified halloysites

Samples	T (°C)	First region				Second region				First region		Second region			
		A (mg g^{-1} min^{-2})	B (mg g^{-1} min^{-1})	C (mg g^{-1})	R^2	A (mg g^{-1} min^{-2})	B (mg g^{-1} min^{-1})	C (mg g^{-1})	R^2	a_1 (mg g^{-1} min^{-2})	v_{01} (mg g^{-1} min^{-1})	t_{02}* (min)	Q_{02}* (mg g^{-1})	a_2 (mg g^{-1} min^{-2})	v_{02} (mg g^{-1} min^{-1})
H	25	−0.092	2.22	1.32	0.88	−0.006	0.70	8.46	0.77	−0.18	1.68	47.97	15.26	−0.012	0.13
	40	0.026	0.37	3.36	0.82	−0.004	0.53	5.45	0.94	0.05	1.14	46.53	9.45	−0.008	0.20
	55	−0.016	0.66	3.00	0.65	−0.002	0.43	4.54	0.97	−0.03	1.01	41.10	7.48	−0.005	0.18
H600	25	0.035	0.49	5.89	0.76	−0.013	1.32	6.39	0.86	0.07	1.82	33.08	14.71	−0.026	0.46
	40	−0.015	0.87	3.51	0.80	−0.011	1.29	0.72	0.91	−0.03	1.45	29.72	11.74	−0.022	0.40
	55	−0.084	1.60	0.27	0.99	-7.1×10^{-6}	0.42	4.30	0.84	-1.43×10^{-5}	0.99	11.92	4.65	−0.168	0.39
H600-5N	25	−0.400	7.58	3.01	0.82	−0.010	0.13	50.36	0.64	−0.80	5.24	18.42	46.08	−0.002	0.17
	40	−0.470	8.60	0.38	0.93	−0.004	0.41	36.04	0.81	−0.94	4.23	36.04	39.89	−0.007	0.15
	55	−0.107	3.79	3.99	0.89	−0.006	0.59	24.20	0.66	−0.21	3.25	24.20	30.22	−0.011	0.09

*In the first region, t_{01} and Q_{01} values are equal to zero; equilibrium time, te, equal 120 min.

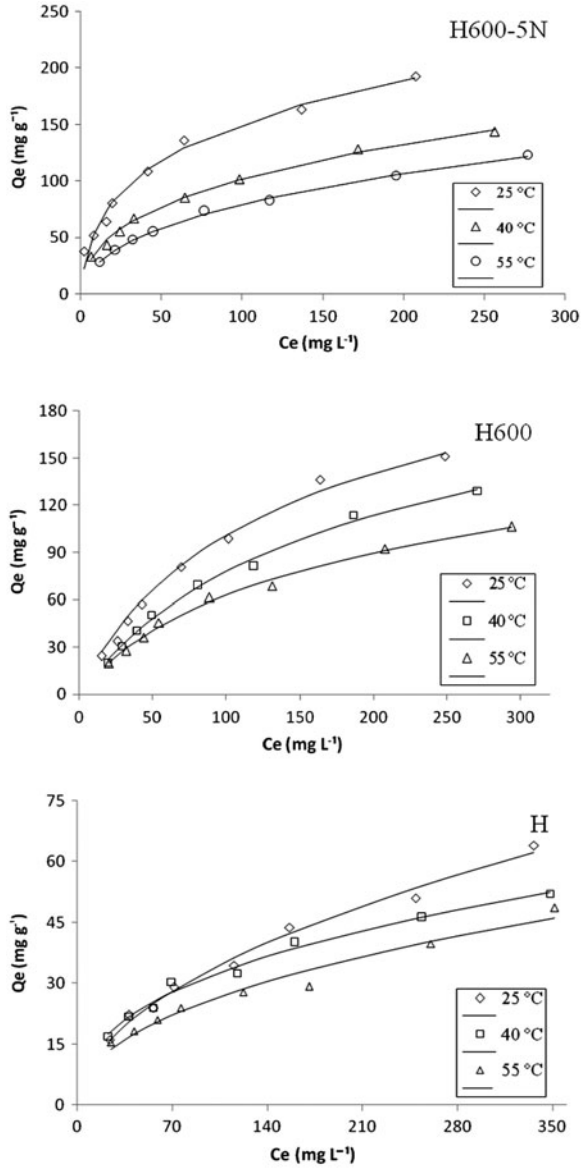

Fig. 5. Adsorption isotherms of MG, according to the experimental data (…) and RP model (—), onto H, H600, and H600-5N.

sawdust, and activated carbon. Thereby, this material appears very effective for removing cationic dyes from wastewaters.

3.2.3.3. Fitting the models to the experimental data. Fitting of adsorption isotherm equations to experimental data is an important aspect of data analysis. The accuracy of the fit of a model with the experimental data is given by the determination coefficient, R^2, which is the square of the correlation coefficient, R, and the average relative error, $E\%$. Sample was eliminated on the basis of a determination coefficient lower than 0.98

Table 5
Comparison of uptake capacities of MG for various adsorbents

Adsorbent	Q_m (mg g^{-1})	Refs.
Neem sawdust	4.3	[11]
Kaolinite	25.7	[38]
Natural zeolite	27.3	[39]
Coconut coir activated carbon	27.4	[13]
Organically modified clay	56.8	[40]
Beech sawdust	83.2	[41]
Bentonite clay	178.6	[42]
H600-5N	192.6	Present study

and an average relative error higher than 10%. The linearization parameters of both Langmuir and Freundlich models are summarized in Table 6.

The Langmuir isotherm (Eq. (7)) shows an inadequate fit of the experimental data of H and H600-5N, giving E and R^2 values as high as 16.0% and lower than 0.93, respectively. The low representativeness of this model with respect to the experimental data of H600-5N can be explained from its hypotheses: an adsorbent where all sites are identical and energetically equivalent seems to be unlikely for a heat-treated and acid-leached sample. A relatively better description was obtained by Freundlich equation (Eq. (8)), a model applicable for heterogeneous adsorbents. The E values are lower than 10% though some R^2 are <0.98. This feature indicates that adsorption takes place onto energetically heterogeneous solids. This equation was found to be appropriate for describing the MG adsorption onto fly ash [43].

The RP model includes three adjustable parameters and requires a non-linear regression method. It can be applied to both homogeneous and heterogeneous systems. The related parameters are calculated and tabulated in Table 6. The RP equation (Eq. (9)) describes efficiently the MG adsorption onto H, H600, and H600-5N (Fig. 5). The validation parameters of this model were found to be ≥0.98 and <9%. The RP equation was successfully used for the adsorption of Cu(II) onto acetate-intercalated halloysites [44] and Reactive Black 5 onto dolomitic solids [45]. The values of β exponent are <1, indicating a favorable adsorption onto heterogeneous materials. The surface heterogeneity factor, β, depends on the surface properties. Thermal and/or acid activation results in the formation of an amorphous mesoporous texture, which is at the origin of the creation of heterogeneous adsorption sites. H600-5N presents the highest K_{RP} value, in line with its greatest adsorption capacity.

3.2.4. Thermodynamic parameters

The thermodynamic parameters obtained from Eqs. (10)–(12) are listed in Table 7. The negative ΔH° values indicate that the MG adsorption is exothermic. The process is, thus, disadvantaged by an increase in temperature, while the heat release decreases according to:

Table 6
Adjustable parameters of the Langmuir, Freundlich, and RP models

		Langmuir model				Freundlich model				Redlich–Peterson model				
Samples	T (°C)	Q_m (mg g^{-1})	K_L (L mg^{-1})	R^2	E (%)	K_F (L g^{-1})	n	R^2	E (%)	K_{RP} (L g^{-1})	β	a_{RP} (mg $L^{-1})^{-\beta}$	R^2	E (%)
H	25	85.5	0.007	0.953	8.95	3.35	1.99	0.989	4.09	12.041	0.503	3.426	0.990	3.92
	40	61.7	0.013	0.983	7.46	4.85	2.44	0.984	3.69	15.311	0.614	2.769	0.986	3.54
	55	57.5	0.009	0.923	10.89	3.93	2.42	0.974	4.29	11.017	0.561	3.105	0.978	5.47
H600	25	244.0	0.0069	0.985	3.48	4.01	1.46	0.980	8.00	2.115	0.874	0.020	0.995	6.97
	40	213.0	0.0057	0.980	3.88	2.97	1.44	0.976	2.19	1.286	0.942	0.009	0.994	4.21
	55	151.0	0.0075	0.988	3.35	3.70	1.66	0.981	5.63	1.304	0.819	0.025	0.994	3.63
H600-5N	25	208.0	0.035	0.979	16.01	26.68	2.71	0.979	6.12	19.077	0.719	0.425	0.984	8.25
	40	164.0	0.0220	0.984	8.88	15.03	2.43	0.993	3.35	18.534	0.647	0.873	0.996	3.52
	55	145.0	0.0150	0.980	7.52	9.62	2.19	0.996	2.60	9.393	0.623	0.614	0.998	1.44

Table 7
Thermodynamic parameters for the MG adsorption onto modified halloysites

Samples	ΔH (kJ mol^{-1})	ΔS (J mol^{-1} K^{-1})	ΔG (kJ mol^{-1})			R^2
			25°C	40°C	55°C	
H	−4.93	−23.36	2.04	2.39	2.74	0.721
H600	−14.31	−45.33	−0.80	−0.12	0.56	0.997
H600-5N	−27.44	−80.48	−3.45	−2.25	−1.04	0.997

H600-5N > H600 > H. The negative values of ΔS° suggest adsorbate–adsorbent systems much more ordered, for which the number of freedom degrees at the solid–liquid interface decreases with adsorption. The stronger the heat release, the greater ΔS° value. Generally, the change in free energy, for physisorption, is between −20 and 0 kJ mol^{-1}, while chemisorption is from −80 to −400 kJ mol^{-1} [46]. The values of ΔG° show that the MG retention is of physical nature. The adsorption onto H600-5N also occurs spontaneously. Negative values of ΔG° were also found for the MG-modified kaolin system [47]. This spontaneous character decreases with increasing temperature. For H600, the process becomes not spontaneous at 55°C. The negative values of ΔH° and ΔS°, associated with the positive values of ΔG°, indicate that, for H, adsorption would be spontaneous at low temperatures [48].

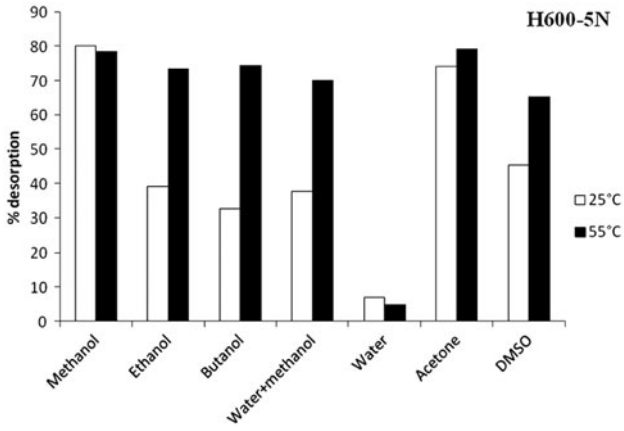

Fig. 6. Desorption percentage of MG from H600-5N with different solvents, at 25 and 55°C.

3.3. Desorption and regeneration

The heat-treated and acid-leached sample (H600-5N) presents the strongest adsorption capacity towards MG. It was, thus, considered for the desorption and regeneration studies. Seven solvents and two temperatures were used to extract MG adsorbed onto H600-5N (Fig. 6). Desorption and regeneration values give an idea about the type of the adsorbate–adsorbent interaction, and the possibility of adsorbent regeneration [49]. Water is a very poor regenerant, since only 6.88% were desorbed at 25°C from H600-5N. This proves that MG has more affinity for this material than for water. Among the other eluents, methanol manifests at 25°C the greatest desorption capacity. This capacity is very sensitive with respect to the length of hydrocarbon chain, i.e., methanol, ethanol, and butanol. The longer the hydrocarbon chain, the lower the desorption capacity. At 25°C, methanol desorbs 80.0% of the total amount adsorbed. If the adsorption process is entirely reversible, 100% of the adsorbed molecules will be desorbed. The fact to obtain 80% indicates that some heterogeneity exists on the surface of the halloysitic solid, where a strong interaction is possible between MG molecules and some sites of higher energy [50].

Desorption increases overall with temperature, i.e. at 55°C instead of 25°C. It reaches an extent more or less identical, around 75%, except for water. This could be explained by the physical nature of the MG adsorption onto H600-5N (ΔH = −27.44 kJ mol^{-1}). It would be expected that an increase in temperature would result in an increase in desorption rate, due to decreasing adsorption capacity. Whatever temperature, the recovered dye was characterized at λ_{max} of 617 nm, i.e. the same wavelength considered in adsorption. This confirms that there is no change in MG structure during recovery process [51].

The ease in desorption and regeneration constitutes an important aspect for the practical application of any adsorbent. Six adsorption–desorption cycles were evaluated using methanol as eluent (Fig. 7). In the first four cycles, H600-5N maintains almost the same adsorption capacity. From the fifth cycle, it decreases and reaches 61%, for the last cycle. One of the met problems is that a certain amount of the adsorbent was lost during the successive adsorption–desorption cycles. Another problem is that some adsorption sites were occupied permanently by alcohol [52]. This explains why from a certain number of cycles, adsorption decreases.

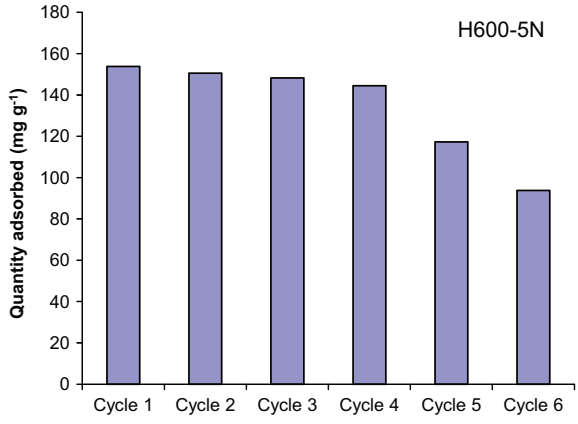

Fig. 7. Adsorption capacity of H600-5N according to the successive cycles at 25°C.

4. Conclusion

Thermal and acid treatments lead to a halloysitic solid having promising adsorptive properties. Halloysite was, thus, treated at 600°C and with 5-N HCl. The obtained solid, H600-5N, maintains its nanotubular structure, leaches Al from octahedral sheet, presents a SiO_2/Al_2O_3 molar ratio of 27.11, develops a microporosity of 20.3%, and highlights a specific area of 503 $m^2\ g^{-1}$. As consequence, it adsorbs 192.6 mg g^{-1} of MG at 25°C. This adsorption is spontaneous and exothermic, i.e. of physical nature. MG is easily desorbed with methanol. H600-5N is easily regenerated and maintains its adsorption capacity within four adsorption–desorption cycles. On the basis of all these considerations, this material may be used as a viable adsorbent for dye removal from the effluents of textile and allied industries.

References

[1] M. Asgher, Biosorption of reactive dyes: A review, Water Air Soil Pollut. 223 (2012) 2417–2435.
[2] G. Crini, Non-conventional low-cost adsorbents for dye removal: A review, Bioresour. Technol. 97 (2006) 1061–1085.
[3] R. Ahmad, R. Kumar, Adsorption studies of hazardous malachite green onto treated ginger waste, J. Environ. Manage. 91 (2010) 1032–1038.
[4] S. Srivastava, R. Sinha, D. Roy, Toxicological effects of malachite green, Aquat. Toxicol. 66 (2004) 319–329.
[5] M.A. Rauf, S.S. Ashraf, Survey of recent trends in biochemically assisted degradation of dyes, Chem. Eng. J. 209 (2012) 520–530.
[6] P. Bansal, N. Bhullar, D. Sud, Studies on photodegradation of malachite green using TiO_2/ZnO photocatalyst, Desalin. Water Treat. 12 (2009) 108–113.
[7] C. Bai, W. Xiao, D. Feng, M. Xian, D. Guo, Z. Ge, Y. Zhou, Efficient decolorization of malachite green in the Fenton reaction catalyzed by [Fe(III)-salen]Cl complex, Chem. Eng. J. 215–216 (2013) 227–234.
[8] L.W. Man, P. Kumar, T.T. Teng, K.L. Wasewar, Design of experiments for malachite green dye removal from wastewater using thermolysis—Coagulation–flocculation, Desalin. Water Treat. 40 (2012) 260–271.
[9] M. Küçükosmanoğlu, O. Gezici, A. Ayar, The adsorption behaviors of methylene blue and methyl orange in a diaminoethane sporopollenin-mediated column system, Sep. Purif. Technol. 52 (2006) 280–287.
[10] H. Mittal, V. Parashar, S.B. Mishra, A.K. Mishra, Fe_3O_4 MNPs and gum xanthan based hydrogels nanocomposites for the efficient capture of malachite green from aqueous solution, Chem. Eng. J. 255 (2014) 471–482.
[11] S.D. Khattri, M.K. Singh, Removal of malachite green from dye wastewater using neem sawdust by adsorption, J. Hazard. Mater. 167 (2009) 1089–1094.
[12] O.S. Bello, M.A. Ahmad, Coconut (*Cocos nucifera*) shell based activated carbon for the removal of malachite green dye from aqueous solutions, Sep. Sci. Technol. 47 (2012) 903–912.
[13] Uma, S. Banerjee, Y.C. Sharma, Equilibrium and kinetic studies for removal of malachite green from aqueous solution by a low cost activated carbon, J. Ind. Eng. Chem. 19 (2013) 1099–1105.
[14] K. Farhadi, A.A. Matin, P. Hashemi, Removal of malachite green from aqueous solutions using molecularly imprinted polymer, Desalin. Water Treat. 24 (2010) 20–27.
[15] F. Bergaya, B.K.G. Theng, G. Lagaly (Eds.), Handbook of Clay Science Developments in Clay Science, vol. 1, Elsevier, Amsterdam, 2006.
[16] S. Mellouk, S. Cherifi, M. Sassi, K. Marouf-Khelifa, A. Bengueddach, J. Schott, A. Khelifa, Intercalation of halloysite from Djebel Debagh (Algeria) and adsorption of copper ions, Appl. Clay Sci. 44 (2009) 230–236.
[17] S. Kadi, S. Lellou, K. Marouf-Khelifa, J. Schott, I. Gener-Batonneau, A. Khelifa, Preparation, characterisation and application of thermally treated Algerian halloysite, Micropor. Mesopor. Mater. 158 (2012) 47–54.
[18] K. Marouf-Khelifa, A. Khelifa, A. Belhakem, R. Marouf, F. Abdelmalek, A. Addou, The adsorption of pentachlorophenol from aqueous solutions onto exchanged Al-MCM-41 materials, Adsorpt. Sci. Technol. 22 (2004) 1–12.
[19] F. Boucif, K. Marouf-Khelifa, I. Batonneau-Gener, J. Schott, A. Khelifa, Preparation, characterisation of thermally treated Algerian dolomite powders and application to azo-dye adsorption, Powder Technol. 201 (2010) 277–282.
[20] S. Lagergren, Zur theorie der sogenannten adsorption gelöster stoffe (About the theory of so-called adsorption of soluble substances), Kungliga SvenskaVetenskapsademiens, Handlingar (K. Sven. Vetenskapsakad. Handl.) 24 (1898) 1–39.
[21] Y.S. Ho, G. McKay, Pseudo-second order model for sorption processes, Process Biochem. 34 (1999) 451–465.
[22] W.J. Weber, J.C. Morris, Kinetics of adsorption on carbon from solution, J. Sanitary Eng. Div. Am. Soc. Civ. Eng. 89 (1963) 31–59.
[23] B. Samiey, S. Farhadi, Kinetics and thermodynamics of adsorption of fuchsin acid on nickel oxide nanoparticules, Acta Chim. Slov. 60 (2013) 763–773.

[24] I. Langmuir, The adsorption of gases on plane surfaces of glass, mica and platinum, J. Am. Chem. Soc. 40 (1918) 1361–1403.
[25] H.M.F. Freundlich, Over the adsorption in solution, J. Phys. Chem. 57 (1906) 385–470.
[26] O. Redlich, D.L. Peterson, A useful adsorption isotherm, J. Phys. Chem. 63 (1959) 1024–1024.
[27] Y. Deng, G.N. White, J.B. Dixon, Effect of structural stress on the intercalation rate of kaolinite, J. Colloid Interface Sci. 250 (2002) 379–393.
[28] E. Abdullayev, A. Joshi, W. Wei, Y. Zhao, Y. Lvov, Enlargement of halloysite clay nanotube lumen by selective etching of aluminum oxide, ACS Nano 6 (2012) 7216–7226.
[29] J.P. Nguetnkam, R. Kamga, F. Villiéras, G.E. Ekodeck, A. Razafitianamaharavo, J. Yvon, Assessment of the surface areas of silica and clay in acid-leached clay materials using concepts of adsorption on heterogeneous surfaces, J. Colloid Interface Sci. 289 (2005) 104–115.
[30] M. Liu, B. Guo, M. Du, F. Chen, D. Jia, Halloysite nanotubes as a novel β-nucleating agent for isotactic polypropylene, Polymer 50 (2009) 3022–3030.
[31] B.H. Hameed, M.I. El-Khaiary, Malachite green adsorption by rattan sawdust: Isotherm, kinetic and mechanism modeling, J. Hazard. Mater. 159 (2008) 574–579.
[32] P. Luo, Y. Zhao, B. Zhang, J. Liu, Y. Yang, J. Liu, Study on the adsorption of Neutral Red from aqueous solution onto halloysite nanotubes, Water Res. 44 (2010) 1489–1497.
[33] C.P. Sekhar, S. Kalidhasan, V. Rajesh, N. Rajesh, Bio-polymer adsorbent for the removal of malachite green from aqueous solution, Chemosphere 77 (2009) 842–847.
[34] S. Boutemedjet, O. Hamdaoui, Sorption of malachite green by eucalyptus bark as a non-conventional low-cost biosorbent, Desalin. Water Treat. 8 (2009) 201–210.
[35] N.K. Kannan, M.M. Sundaram, Kinetics and mechanism of removal of methylene blue by adsorption on various carbons—A comparative study, Dyes Pigm. 51 (2001) 25–40.
[36] K. Belkassa, F. Bessaha, K. Marouf-Khelifa, I. Batonneau-Gener, J.D. Comparot, A. Khelifa, Physicochemical and adsorptive properties of a heat-treated and acid-leached Algerian halloysite, Colloids Surf., A 421 (2013) 26–33.
[37] C.H. Giles, T.H. MacEwan, S.N. Nakhwa, D. Smith, Studies in adsorption. Part XI. A system of classification of solution adsorption isotherms, and its use in diagnosis of adsorption mechanisms and in measurement of specific surface areas of solids, J. Chem. Soc. 60 (1960) 3973–3993.
[38] E. Castellini, R. Andreoli, G. Malavasi, A. Pedone, Deflocculant effects on the surface properties of kaolinite investigated through malachite green adsorption, Colloids Surf., A 329 (2008) 31–37.
[39] R. Han, Y. Wang, Q. Sun, L. Wang, J. Song, X. He, C. Dou, Malachite green adsorption onto natural zeolite and reuse by microwave irradiation, J. Hazard. Mater. 175 (2010) 1056–1061.
[40] S. Arellano-Cárdenas, S. López-Cortez, M. Cornejo-Mazón, J.C. Mares-Gutiérrez, Study of malachite green adsorption by organically modified clay using a batch method, Appl. Surf. Sci. 280 (2013) 74–78.
[41] A. Witek-Krowiak, Analysis of influence of process conditions on kinetics of malachite green biosorption onto beech sawdust, Chem. Eng. J. 171 (2011) 976–985.
[42] E. Bulut, M. Özacar, İ.A. Şengil, Adsorption of malachite green onto bentonite: Equilibrium and kinetic studies and process design, Micropor. Mesopor. Mater. 115 (2008) 234–246.
[43] S. Dubey, Uma, L. Sujarittanonta, Y.C. Sharma, Application of fly ash for adsorptive removal of malachite green from aqueous solutions, Desalin. Water Treat. 53 (2015) 91–98, doi: 10.1080/19443994.2013.846552.
[44] S. Mellouk, A. Belhakem, K. Marouf, J. Schott, A. Khelifa, Cu(II) adsorption by halloysites intercalated with sodium acetate, J. Colloid Interface Sci. 360 (2011) 716–724.
[45] S. Ziane, K. Marouf-Khelifa, H. Benmekki, J. Schott, A. Khelifa, Removal of a reactive textile azo dye by dolomitic solids: Kinetic, equilibrium, thermodynamic, and FTIR studies, Desalin. Water Treat., doi: 10.1080/19443994.2014.941308.
[46] M.J. Jaycock, G.D. Parfitt, Chemistry of Interfaces, Ellis Horwood, Onichester, 1981.
[47] A.C. Suwandi, N. Indraswati, S. Ismadji, Adsorption of N-methylated diaminotriphenilmethane dye (malachite green) on natural rarasaponin modified kaolin, Desalin. Water Treat. 41 (2012) 342–355.
[48] W.L. Masterton, C.N. Hurley, Chemistry: Principles and Reactions, fifth ed., Brooks/Cole, California, CA, 2003.
[49] G. McKay, G. Ramprasad, P. Mowli, Desorption and regeneration of dye colours from low-cost materials, Water Res. 21 (1987) 375–377.
[50] M.I. El-Barghouthi, A.H. El-Sheikh, Y.S. Al-Degs, G.M. Walker, Adsorption behavior of anionic reactive dyes on H-type activated carbon: Competitive adsorption and desorption studies, Sep. Sci. Technol. 42 (2007) 2195–2220.
[51] C. Kannan, T. Sundaram, T. Palvannan, Environmentally stable adsorbent of tetrahedral silica and non-tetrahedral alumina for removal and recovery of malachite green dye from aqueous solution, J. Hazard. Mater. 157 (2008) 137–145.
[52] J.M. Chern, C.Y. Wu, Desorption of dye from activated carbon beds: Effects of temperature, pH, and alcohol, Water Res. 35 (2001) 4159–4165.